Autonomous shipborne in situ reflectance data in optically complex coastal waters for validation of Sentinel-3 imagery: a case study of the Salish Sea, Canada

Ziwei Wang[a] and Maycira Costa[a]

[a] Department of Geography, University of Victoria, Victoria, Canada

1 Introduction

Ocean colour satellite sensors are a practical approach for providing large-scale synoptic monitoring of aquatic environments (Simis & Olsson, 2013). For instance, spectral reflectance features are used to retrieve bio-optical variables such as chlorophyll concentration (i.e., the direct proxy for phytoplankton biomass) and seawater inherent optical properties (IOPs) (Kirk, 1995). However, this capability is accomplished through the determination of water-leaving radiance which is extracted from top of atmosphere (TOA) radiances measured by satellite sensors using atmospheric correction algorithms (Müller et al., 2015). Given that the atmospheric signal comprises about 80% or more of the total measurement by satellite sensors at TOA, it needs to be removed to isolate the signal from the ocean, for successful retrieval of the biogeochemical properties of water bodies (Müller et al., 2015). Thus, a priori knowledge of the in situ above water reflectance of the water body in the absence of an intervening atmosphere can be an effective reference point for validation of satellite-derived atmospheric corrected reflectance (Simis & Olsson, 2013). Reflectance measured by above-water radiometers from stationary (Zibordi et al. 2004, 2009) or moving platforms can aid the calibration and validation of satellite-derived reflectance due to increased match-ups. However, automated methods to evaluate *in situ* spectra quality are required before comparison with satellite data. For example, precipitation, cloud conditions (Lewis, 2008), shadow and ship superstructure negatively influence the measure spectra signals (Hooker & Morel, 2003).

The objectives of this research were (1) to develop a framework for acquisition, quality control, including meteorological flags and superstructure signal, and consider three different approaches for deriving above-water remote sensing reflectance acquired with autonomous sensors - SAS Solar Tracker, installed aboard the Queen of Oak Bay Ferry, west coast of Canada; and (2) to use SAS-derived $R_{rs}(\lambda)$ to validate Sentinel-3-atmospherically corrected $R_{rs}(\lambda)$ derived from different methods, Polymer 4.8, and C2RCC 0.15.

2 Approach: data acquisition

We installed a set of hyperspectral radiometers on a commercial ferry, the BC ferry's Queen of Oak Bay, to measure radiances and irradiance with solar tracking capability that permits autonomous operation (SAS Solar Tracker, or Ferry Ocean Colour Observation System, FOCOS). The FOCOS system consists of two hyperspectral radiometers to measure sea surface radiance ($L_t(\lambda)$), sky radiance ($L_i(\lambda)$), and a third sensor to measure total irradiance ($E_s(\lambda)$); from these measurements, remote sensing reflectance, $R_{rs}(\lambda)$, is derived. FOCOS was installed on a white ferry, 19 meters above the water surface, with considerations to avoid infrastructure shadows (calculated at approximately 11m from the ship wall at spring/summer time), spray, and sun glint. Specifically, $L_t(\lambda)$ and $L_i(\lambda)$ are at a fixed viewing zenith angle, $\theta v = 50^o$, and viewing-sun azimuth, $\phi v = 120^o$ to avoid the effects of glint (Hooker & Morel, 2003). The ideal ϕv is maintained using an autonomous steeper motor platform that triggers the required positioning according to ship heading and sun azimuth (Satlantic Inc).

The data acquired from the 12:50 to 14:30 ferry run from Departure Bay to Horseshoe Bay during the spring and summer of 2016 was selected as it is closest to the satellite overpass. An accompanying ferry box system measured salinity, chla, CDOM, and turbidity information at the same time and location. Additionally, a benchtop sampling method was used for measuring total and dissolved organic matter absorption, scattering, and backscattering with the ac-S meter. Before and after each data collection cruise, the ac-S was calibrated

using DI water in a laboratory setting to account for any instrument drift (Twardowski et al., 1999). The ac-S and BB3 data were further used in the method by Groetsch et al. (2017).

3 Data processing: approach and results

Data from FOCOS was processed with our open source application PySciDON (Python Scientific framework for Development of Ocean Network applications). PySciDON was designed using a Model-View-Controller (MVC) design pattern, with a framework for processing large amounts of in situ radiance and irradiance data acquired with autonomous sensors aboard ships. PySciDON has multiple levels of processing, considering calibration of radiance and irradiance data, flags for erroneous acquisition angles, latitude and longitude directional errors, and environmental conditions (sun elevation, clouds, and rain), $R_{rs}(\lambda)$ calculation, and simulation of $R_{rs}(\lambda)$ for specific satellite bands (Vandenberg et al., 2017).

Meteorological flags: clouds and rain

For this analysis, approximately 35,000 *in situ* spectra were measured at different meteorological conditions between about 13:00 and 14:30 pm from June 18th to July 13th with the FOCOS system. All the measured *in situ* spectra were averaged every 1 minute, which resulted in about 1,400 averaged spectra. Additionally, two cameras were installed on the spectrometer to acquire the images of the sky, and water surface and humidity data (acquired with a RM Young Temperature RH 41382VC-L 27306), all at 1-minute intervals. Weather conditions were determined based on the evaluation of the sky images, which were classified into seven categories: rainy, overcast, variable clouds (merged 100%, 75% and 50% cloudy conditions), and sunny (merged 25% cloudy and sunny). We defined the following meteorological flags, adapted from Wernand (2002):

Flag 1 $E_s(\lambda = 480\ nm) > 2\ u\ W \cdot cm^{-2} \cdot nm^{-1}$: selecting significant Es.

Flag 2 $E_s(\lambda=470nm)/E_s(\lambda=680\ nm)>1$: masking spectra acquired at dawn/dusk

Flag 3 $E_s(\lambda = 720\ nm) / E_s(\lambda = 370\ nm)$: masking spectra affected by rainfall and high humidity.

Based on the defined classification scheme, the analysis showed that the flags accurately identified rainy (97.6% accuracy), overcast (76.4%) and sunny (98.5%) weather conditions, and they were then implemented in PySciDON as part of our operational analysis of valid spectra.

Reflectance calculation

Following the application of meteorological flags and any other inconsistency on data quality, three methods were applied to calculate water reflectance based on the measured radiances and irradiance.

(i). Mobley (1999) (R_{rs}^{M99}): The remote sensing reflectance is defined as the ratio between water-leaving radiance (L_w) and total irradiance (E_s): $R_{rs}^{M99}(\lambda) = \frac{L_t(\lambda) - \rho_s L_i(\lambda)}{E_s(\lambda)}$ Equation (1). Where L_t is the measured total radiance by the sea viewing sensor corresponding to $L_t(\lambda) = L_w(\lambda) + \rho_s L_i(\lambda)$; ρ_s is the fraction of sky radiance that is measured by the sea viewing sensor (Mobley, 1999). Variable illumination and surface roughness conditions make the determination of ρ_s a challenge. Sky glint is usually less than 5% of the acquired sky radiance (L_i) (Morel & Bricaud, 1981). However, it can have a similar magnitude to L_w, and therefore the choice of ρ_s significantly influences the accuracy of R_{rs} calculations. ρ_s was defined considering the local wind speed measured at Entrance Island and Halibut Bank, following Mobley (1999). The measured wind speed ranged from 0.8 - 10.4 m/s with the corresponding ρ_s ranges from 0.035 to 0.048.

(ii). Mobley (1999) with correction for ship superstructure reflectance ($R_{rs}^{M99+ship}$): In addition to the accurate determination of ρ_s, the ship superstructure (ship wall) influences the above-water radiometry by introducing signal to the radiance field measured by the sea viewing sensor. To quantify the ship superstructure perturbation on the measured radiometry data, measured radiometric data were chosen from the day with

the lowest water reflectance (implying the lowest turbidity) coinciding with high salinity (implying less influence of river plume waters), and as such, we assumed that the infrared reflectance (R_{rs}(780)) was negligible after removing sky glint signal using Mobley, (1999) (Hooker & Morel, 2003). These correspond to approximately 940 measurements. We evaluated $R_{rs}^{M99}(780)$ at different rotator angles (α °) and at azimuth angles between the heading of the ferry and the position of the sun (γ °), to define possible superstructure signal (R_{ship}). From this analysis, we defined that the ship wall was always under non-slit conditions, which minimizes any superstructure reflection onto the water (Hooker & Morel, 2003), and that data acquired at rotator angles lower than - 50° (about 13 m from ship wall) should be removed due to possible measurements of shadowed waters (this was confirmed during field observation). Further, there was no indication of increased reflectance as the rotator angle approximates the ship wall (from -25 to -47^0, corresponding to 18 and 13 m from the ship wall, respectively) (Figure 1a).

Figure 1b shows the histogram of $R_{rs}^{M99}(780)$ values, with the median value corresponding to 6.1262 [sr^{-1}] and a standard deviation value of 0.3538 [sr^{-1}] (after removal of glint and shadow contaminated data). From this, the value corresponding to the superstructure reflectance (R_{ship}=R_{rs}^{M99} (780)) was defined as the median – 2 x SD, corresponding to 5.4186 *10^{-4} [sr^{-1}]. Adapted from preview work by Hooker & Morel (2003), a wavelength dependent radiance from a white ship, $L_{ship}(\lambda)$, measured as part of L_t, can be written as $L_{ship}(\lambda) = [L_t(780) - \rho_s L_i(780)]\frac{E_d(\lambda)}{E_d(780)}$ (Equation 2). Equation (2) can also be written as $L_{ship}(\lambda) = R_{rs}^{M99}(780)E_d(\lambda)$ (Equation 3). At any wavelength, $R_{rs}(\lambda)$ can be calculated as $R_{rs}(\lambda) = \frac{L_t(\lambda)-\rho_s L_i(\lambda)-L_{ship}(\lambda)}{E_d(\lambda)}$ (Equation 4) or $R_{rs}(\lambda) = \frac{L_t(\lambda)-\rho_s L_i(\lambda)}{E_d(\lambda)} - R_{rs}^{M99}(780)$ (Equation 5). $R_{rs}^{M99}(780)$ is the constant we quantified as the ship contributed reflectance (R_{ship}) base on analysis of the clearest water with the lowest reflectance at 780 nm. Thus, Equation 4 can be written as $R_{rs}^{M99+ship}(\lambda) = \frac{L_t(\lambda)-\rho_s L_i(\lambda)}{E_d(\lambda)} - R_{ship}$ (Equation 6), where R_{ship} = 5.4186 *10^{-4} [sr^{-1}] for our case and should vary for a different ship superstructure environment.

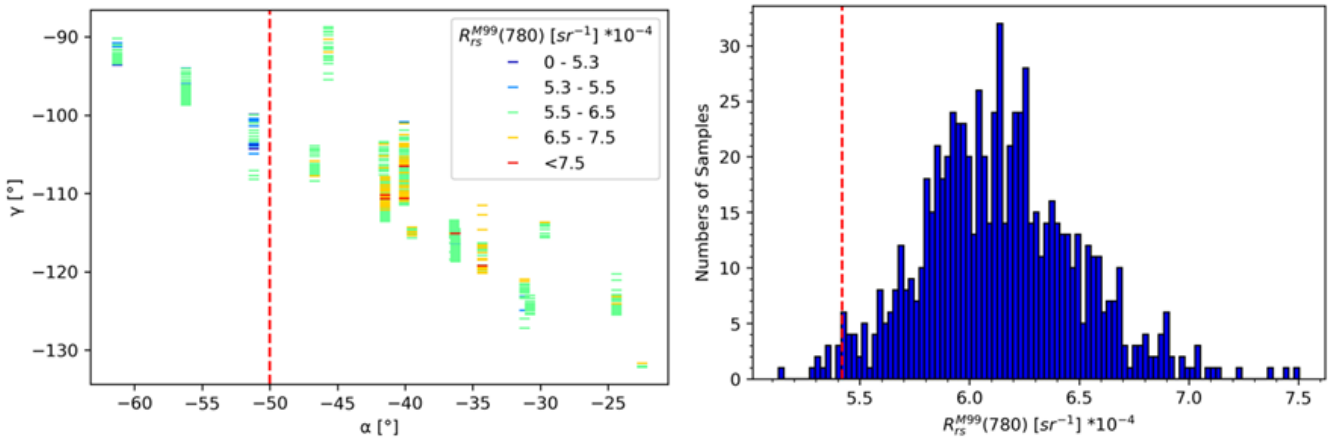

Figure 1: a) $R_{rs}^{M99}(780)$ values for July 06, 2016 and its rotator angle (α °) and ferry heading and sun azimuth angle (γ °) at the time of measurement. The red dashed line indicates the threshold value for shadow. b) The histogram $R_{rs}^{M99}(780)$ for the same dataset. The red dashed line indicates the threshold determined to represent superstructure contributed reflectance (R_{ship}).

(iii) 3C approach provided by Groetsch et al., 2017(R_{rs}^{3C}):

FOCOS data was also processed with a three-component reflectance model (3C) from Groetsch et al. (2017), which estimates a spectrally resolved offset $\Delta(\lambda)$ to correct for residual sun and sky glint, applicable to above-water measurement, and independent of ρ_s. The model is tuned using ac-S measured local S_{CDOM}=0.0155, a_{CDOM} with a start value at 0.525 m^{-1} and range from 0.007 to 3.0 m^{-1}. Backscattering data is also provided externally from BB3 measurement.

Sentinel-3 image processing

Level 1 Sentinel-3 images were processed with Polymer 4.8, C2RCC 0.15, and the standard ESA Level 2 water leaving reflectance products. A total of 15 images with corresponding 750 match ups with FOCOS in situ Rrs measured (averaged within 90 seconds) were analyzed. Each in situ R_{rs} corresponds to a 3x3 Sentinel-3 image match up window. After deleting the adjacency contaminated samples and mismatch samples in the boundary of ocean and plume water, 358 ocean and 243 plume samples were kept for further analysis.

4 Sentinel-3 reflectance validation

Figure 2 shows the relationship between in situ FOCOS $R_{rs}^{M99+ship}$ and Sentinel 3-derived R_{rs} at 560 nm according to different processing methods, Polymer v2.8, C2RCC, and standard ESA Level 2. Note that, generally, Polymer retrieves R_{rs} closer to the 1:1 line, while ESA Level 2 performs poorly, including negative R_{rs} values, and C2RCC R_{rs} saturated at around 0.03 sr^{-1}. This saturation is caused by a large coccolithophore bloom on Aug 22 and Aug 23, 2016. After deleting those saturation points, statistical analysis was performed considering 358 and 205 ocean (higher salinity) and plume (lower salinity) water samples, respectively.

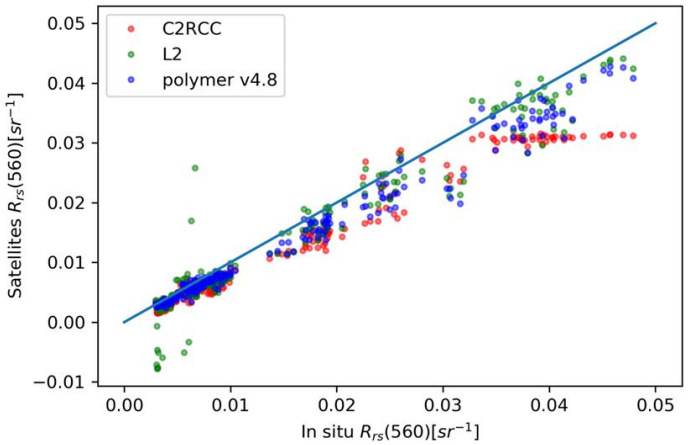

Figure 2: Matchups of C2RCC v0.15, L2 and Polymer v4.8 processed satellite reflectance at 560 nm with corresponding in situ $R_{rs}^{M99+ship}$ for 243 plume water samples. The blue line indicates the 1-to-1 relationship.

The statistical analysis was performed separately for the two groups of waters aiming to identify the improved performance of the considered processing methods, Polymer 4.8, C2RCC 0.15, and the standard ESA Level 2. In our dataset, ocean waters showed chla 0.5-5 µg/l, turbidity 1.6-8.0 NTU and 5.0-24.0 (coccolithophores bloom), and CDOM 1.5-3.0; plume water showed chla 0.6-5.5, turbidity 1.6-7.0 NTU and 4.0-25.0 (coccolithophores bloom), and CDOM 2.0-6.0. Before the statistical analysis, a detailed investigation regarding the match-up quality of the dataset was conducted to guarantee that good matchups correspond to the same water mass sampled by FOCOS and Sentinel-3. The Salish Sea is a dynamic water system under the influence of a large river plume, the Fraser River, tides and currents. A dataset, composed of ferrybox biogeochemical (chla, CDOM, and turbidity) and CODAR data, allowed for a robust spatiotemporal traceability of the uncertainties associated with the quality of matchups in the interface of the Fraser River plume and ocean waters. This analysis revealed that the uncertainties of the poor-quality match ups were a function of the local current speed and direction and heterogeneity of water masses, adding to large uncertainties between Sentinel-derived R_{rs} and FOCOS-derived R_{rs}; the poor-quality match ups were removed from further analysis.

Figure 3 shows a summary of the final statistics for the different methods, for ocean and plume waters. For the ocean water, the best performance was achieved with Polymer- derived R_{rs} when compared with in situ $R_{rs}^{M99+ship}$. Correlation coefficients (r) were > 0.9 and the mean absolute percentage difference (MAD) ranged from 12-39% (highest deviation always for the 400nm band) for the Sentinel-3 visible bands. The C2RCC method showed the second-best performance, especially when compared with the R_{rs}^{3C} (r ranged from 0.7 to

09; MAD ranged from 20 to 80%). The poorest observed performance was for the standard ESA Level 2 R_{rs}, which exhibited the highest uncertainties for all bands (MAD ranging from 36 to 165%), as a result of the poorest correlation across all bands (Figure 3). Similar results were observed for plume waters, where the Polymer showed the best performance, especially when compared with $R_{rs}^{M99+ship}$ (r>0.9; MAD range from 11-30%), and again, the weakest performance was for standard ESA Level 2.

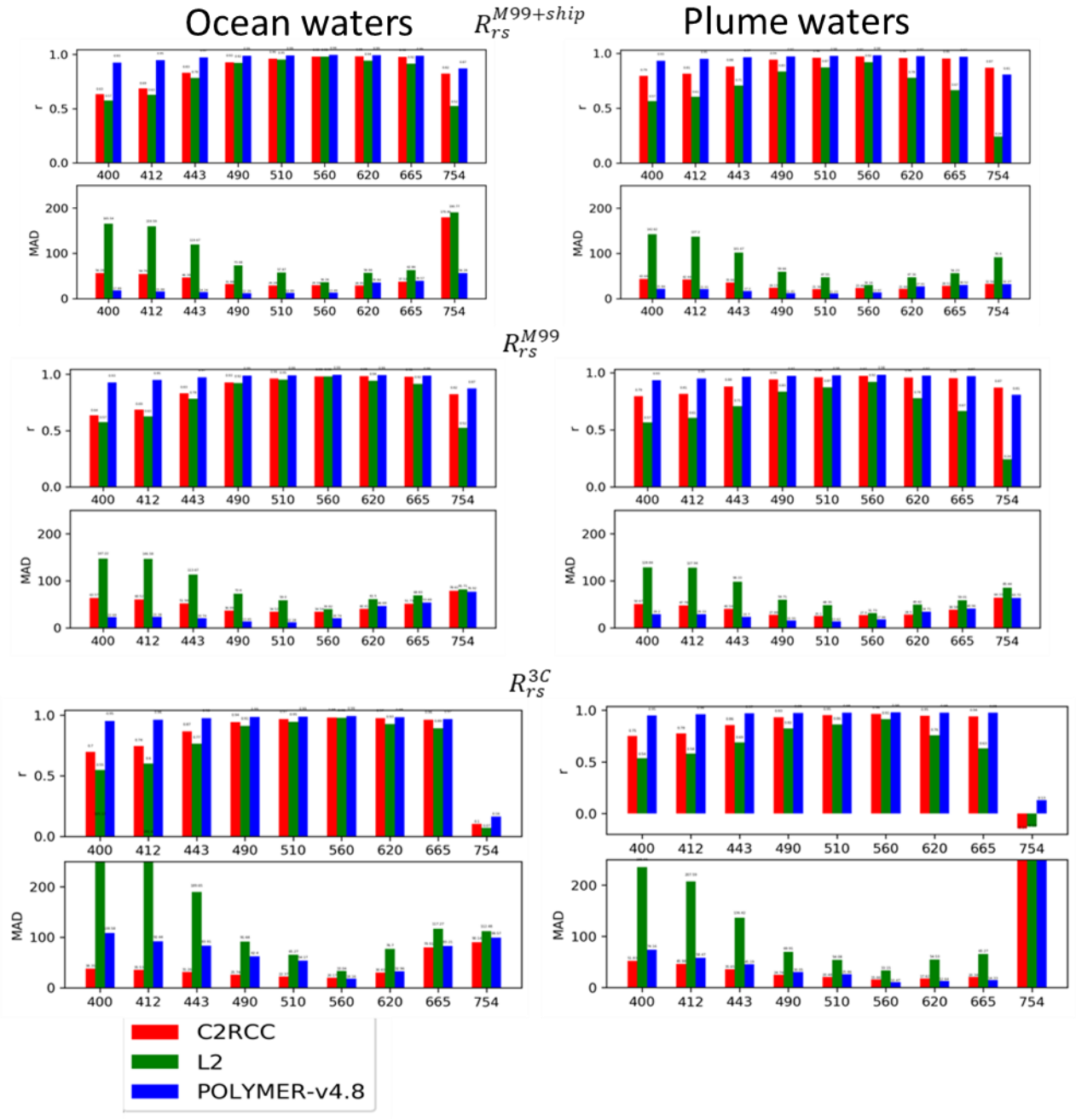

Figure 3. Summary of statistical analysis (correlations coefficient, r, and MAP) of match ups between in situ FOCOS R_{rs} and Sentinel-derived R_{rs} according to different methods.

5 Conclusions

Detailed considerations of installation, meteorological flags, ship shadow, and perturbation related to superstructure albedo were considered to analyze in situ above-water reflectance data acquired with an autonomous solar tracker system installed aboard of a ferry crossing the Salish Sea. The results showed that the defined flags were successful for avoiding data acquired during cloudy or rainy conditions. Ship shadow was defined as present for rotator angles between -50^o and -60^o, based on in situ observations and reflectance values measured at different rotator angles; data acquired at these angles were removed from the analysis. The assumption of null reflectance at 780 nm for our lowest reflectance ocean waters allowed the estimation of a ship superstructure albedo, which was subsequently applied to all the in situ reflectance measurements, considering the in situ total irradiance. R_{ship} = 5.4186 *10^{-4} [sr^{-1}] for our case and should vary for a different ship superstructure environment.

Sentinel-3 processing methods, Polymer, C2RCC, and ESA Level 2, were evaluated (N=590 samples) using in situ FOCOS R_{rs} processed according to (i) wind and geometry related ρ_s, (ii) and an additional correction with R_{ship}, and (iii) a ρ_s independent model. Our results support Polymer as the most appropriate method to determine accurate Sentinel-3 R_{rs}, with r >0.9 and MAP ranging for 11-39% for the OLCI visible bands when compared to FOCOS R_{rs} with correction for ship albedo, for both ocean and plume waters. ESA Level 2 performed the poorest with a general large underestimation of R_{rs} values.

Reference

Doxaran, D., Cherukuru, R. C. N., & Lavender, S. J. (2004). Estimation of surface reflection effects on upwelling radiance field measurements in turbid waters. *Journal of Optics A: Pure and Applied Optics*, *6*(7), 690–697. https://doi.org/10.1088/1464-4258/6/7/006

Garaba, S. P., & Zielinski, O. (2013). Methods in reducing surface reflected glint for shipborne above-water remote sensing. *Journal of the European Optical Society: Rapid Publications*, *8*, 13058. https://doi.org/10.2971/jeos.2013.13058

Hooker, S. B., & Morel, A. (2003). Platform and Environmental Effects on Above-Water Determinations of Water-Leaving Radiances. *Journal of Atmospheric and Oceanic Technology*, *20*(1), 187–205. https://doi.org/10.1175/1520-0426(2003)020<0187:PAEEOA>2.0.CO;2

Kirk, J. (1995). Light and photosynthesis in aquatic ecosystems. *Aquatic Botany*, *50*(1), 111–112. https://doi.org/10.1016/0304-3770(95)90010-1

Mobley, C. D. (1999). Estimation of the remote-sensing reflectance from above-surface measurements. *Applied Optics*, *38*(36), 7442–7455. https://doi.org/10.1364/AO.38.007442

Morel, A., & Bricaud, A. (1981). Theoretical results concerning light absorption in a discrete medium, and application to specific absorption of phytoplankton. *Deep Sea Research Part A. Oceanographic Research Papers*. https://doi.org/10.1016/0198-0149(81)90039-X

Müller, D., Krasemann, H., Brewin, R. J. W., Brockmann, C., Deschamps, P.-Y., Doerffer, R., Fomferra, N.,. Franz, B A., Grant, M.G., Groom, S.B., Mélin, F., Platt,T., Regner, P., Sathyendranath, S., Steinmetz, F., Swinton, J. (2015). The Ocean Colour Climate Change Initiative I: A methodology for assessing atmospheric correction processors based on in-situ measurements. *Remote Sensing Environment*, *162*, 242–256.

Simis, S. G. H., & Olsson, J. (2013). Unattended processing of shipborne hyperspectral reflectance measurements. *Remote Sensing of Environment*, *135*, 202–212. https://doi.org/10.1016/j.rse.2013.04.001

Zibordi, G., Holben, B., Slutsker, I., Giles, D., D'alimonte, D., Mélin, F., Berthon ,J.-F., Vandemark, D., Feng, H., Schuster, G., Fabbri, B.E., Kaitala, S., Seppala, J. (2009). AERONET-OC: A network for the validation of ocean color primary products. *Journal of Atmospheric and Oceanic Technology*, *26*(8), 1634–1651.

Zibordi, G., Mélin, F., Hooker, S. B., Alimonte, D. D., & Holben, B. (2004). An Autonomous Above-Water System for the Validation of Ocean Color Radiance Data, *42*(2), 401–415.